Using Room Temperature Current Noise To Characterize Single Molecular Spectra

Smitha Vasudevan* **and Avik W. Ghosh**

Department of Electrical and Computer Engineering, University of Virginia, Charlottesville, Virginia 22904, United States

ABSTRACT We propose a way to use room temperature random telegraph noise to characterize single molecules adsorbed on a backgated silicon field-effect transistor. The overlap of molecule and silicon electronic wave functions generates a set of trap levels that impose their unique scattering signatures on the voltage-dependent current noise spectrum. Our results are based on numerical modeling of the current noise, obtained by coupling a density functional treatment of the trap placement within the silicon band gap, a quantum kinetic treatment of the output current, and a Monte Carlo evaluation of the trap occupancy under resonance. As an illustrative example, we show how we can extract molecule-specific "fingerprints" of four benzene-based molecules directly from a frequency—voltage colormap of the noise statistics. We argue that such a colormap carries detailed information about the trap dynamics at the Fermi energy, including the presence of correlated interactions, observed experimentally in backgated carbon nanotubes.

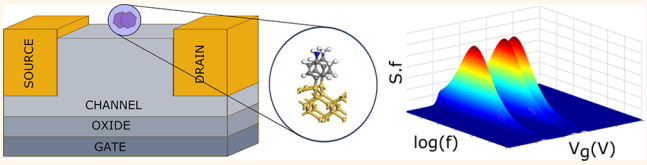

KEYWORDS: random telegraph signals · field-effect transistors · molecule characterization · quantum scattering · correlated traps

The ability to reliably detect trace amounts of molecules is critical to applications in a variety of fields from defense to nanomedicine.[1,2] Recent advances in nanotechnology are opening up the road to accurate, reliable, and portable chemical sensors, which benefit a broad range of industries. The most commonly used sensing devices are chemically modulated field-effect transistors (ChemFETs), typically integrated onto a solid-state platform and working on purely electrostatic principles.[3−5] Upon attachment of a target molecule, there is a transfer of charge that alters the work function of the gate electrode, resulting in a shift in its threshold voltage.[6] Although ChemFETs have their advantages, such as robustness and low cost, they have a few notable challenges, precisely because they operate on long-range electrostatic principles and are thus affected by spurious stray charges in the vicinity. Such false positives become particularly important for nanoscale devices with large surface-to-volume ratios. Also, since the sensing event is characterized by a single entity, that is, a shift in gate threshold voltage for a prefunctionalized device, the results are sensitive to cross-talk between multiple species and are at any rate inapplicable to unknown sample. A more direct detection scheme, where the adsorbates actively participate in the electron conduction process, would be desirable to eliminate such stray detection events.

In this paper, we propose a characterization scheme that uses a *surface-modulated field-effect transistor* (SurFET) and operates on a different detection principle, one that involves stronger chemical bonding between the transistor channel and the adsorbed molecule. The observed output consists of jumps in the current called random telegraph signals (RTS), registered at gate voltage values that are unique to the adsorbate's *in situ* molecular spectrum. One can then compile a library of molecular noise "fingerprints" (Figure 1) from a voltage sweep to determine the location of the traps, which would aid in identifying various molecular species. A frequency—voltage colormap then allows us to extract detailed information about the trap dynamics.

RTS was first observed at low temperatures in metal-oxide-semiconductor field-effect transistors (MOSFETs)[8] and quantum point contact structures[9] and later at room temperature in bipolar transistors.[10] RTS

* Address correspondence to sv4e@virginia.edu.

Received for review August 30, 2013 and accepted January 29, 2014.

Published online January 29, 2014
10.1021/nn404526w

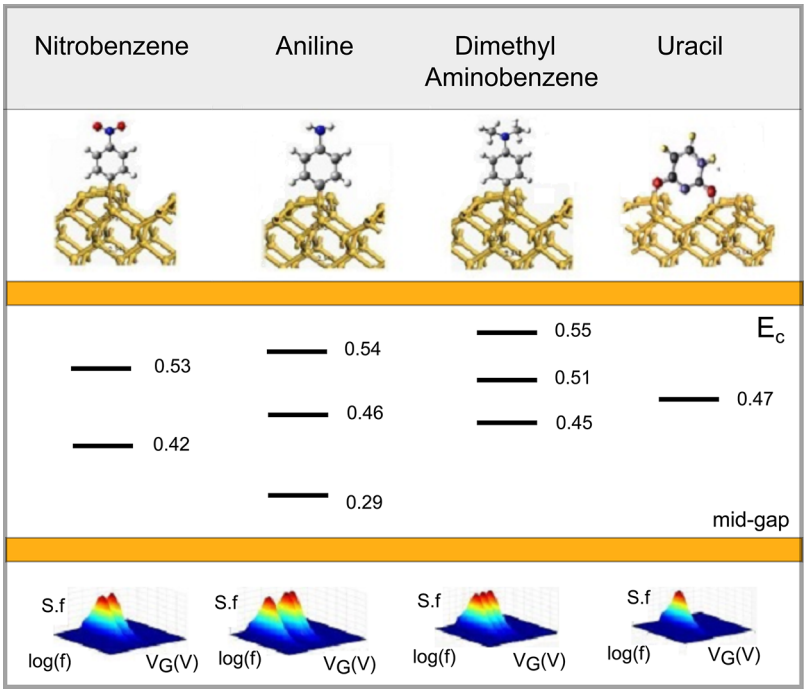

Figure 1. Four molecules studied (top), their calculated RTS power spectral density time frequencies S.f (bottom), and the molecular trap levels (middle) placed from the data within the silicon conduction E_C and valence E_V edges. The data are extracted from conductance−voltage curves, analogous to capacitance−voltage data for deep level transient spectroscopy on electrically active defects.[7] The number and location of the peaks in the power spectrum bear unique fingerprints from individual trap states unique to each molecule.

jumps have since been used to characterize impurity levels in MOSFETs, junction field-effect transistors (JFETs), and carbon nanotube field-effect transistors (CNTFETs).[11] It has now become possible to detect individual impurity effects, culminating in the detection of a single center dangling bond in a commercial transistor,[12,13] and large discrete noise jumps in carbon nanotubes.[14] The RTS from a few traps in nanoscale MOSFETs can now be controlled[15] and activated individually by the gate voltage of nanoscale MOSFETs. More recently, noise spectroscopy has been used as a tool for biosensing in carbon nanotubes[16,17] and silicon nanowire FETs.[18] With the rapid shrinking of device sizes and their improved purities, such effects are expected to be more dominant in the future.

What is striking about these emerging results is their sensitivity to individual scattering events because of the reduced dimension of deeply scaled nanochannels[14] (even one strategically placed impurity can completely block a low-d channel from conducting). The scaled dimension also amplifies the Coulomb costs for charge addition ushering in room temperature RTS, while the rapid field variation in low dimensions near adsorbates allows us to resolve closely spaced trap states. We propose to use the effect not to characterize and eliminate impurities as was done in the 1960s and 1970s but to characterize the actual adsorbates, thereby providing an electronic "barcode" specific to each molecule.

Indeed, we will show that the method gives us an instantaneous snapshot of the system dynamics at the Fermi energy. We will use this approach to validate an earlier hypothesis we made[19] about a unique RTS signature measured in a CNT, which we attributed to the correlated interaction between multiple traps, one blocking the channel and the second unblocking it by blocking the first trap. Our frequency−voltage colormap, extracted from the experimental data, shows a clear smearing of the trap states (Figure 7), indicating the dominance of precisely such a correlated interaction dynamics.

Basic Idea and Design of the SurFET. The basic idea of the SurFET detection mechanism relies on the bonding of the molecule directly to the transistor surface (Figure 2a). An overlap of molecular and semiconductor wave functions serves to passivate existing surface states as well as to create new localized molecular trap levels inside the silicon band gap. Even with thin oxides today, there is significant tunneling, indicating that the wave functions do overlap. A suite of these trap levels bears a unique spectral signature for each adsorbate geometry and can be electronically scanned with a backgate (Figure 2b). Each trap level acts like a Coulomb-blockaded quantum dot; the gate causes electrons to populate or depopulate the dot levels (Figure 2c) near resonance, blocking and unblocking the channel and creating a concomintant flicker in the output current characteristics (Figure 2d). These noise patterns uniquely follow the energy locations of the

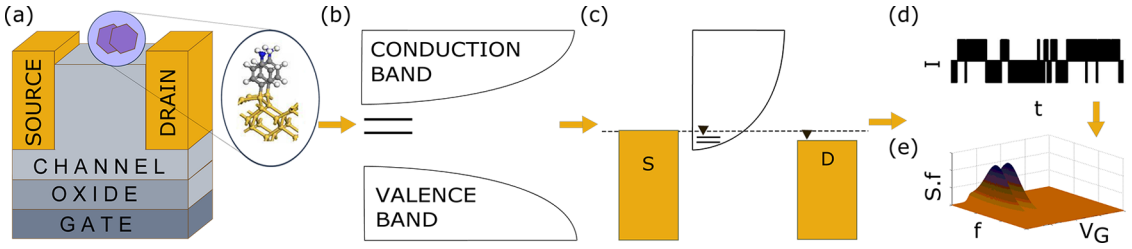

Figure 2. Schematic sequence of events in the characterization protocol, starting with (a) a molecule bonding onto a silicon FET, (b) creating localized trap levels inside the channel band gap. (c) Backgate scans the levels, populating/depopulating them, leading to a blockade-driven (d) random telegraph noise in the current when the gate resonates with the levels. (e) Frequency analysis of this output current shows clear peaks that indicate the location of the traps in the band gap of the silicon–molecule bandstructure. A comparison of this frequency spectrum with the library in Figure 1 gives us the identity of the molecule.

traps, thereby providing a distinctive fingerprint in the current characterisics.

The ensemble of gate voltage windows over which the RTS manifest themselves maps out a molecular barcode that can be compared against a compiled table of theoretical responses to characterize and sense a molecular species (Figure 1). *The significant advantage of such SurFETs is their exclusive detection of only molecules that overlap significantly with the channel to cause a transfer of states*, thereby eliminating false positives. Further refinements include prefunctionalizing the gate with molecules that offer superexchange pathways for direct interaction of the adsorbate with the channel, scaling the channel to amplify variations in the local gate transfer factors, integrating the detector onto a Complementary Metal-Oxide Semiconductor chip, and combining it with other probe techniques such as temperature and field for a more precise characterization.

RESULTS AND DISCUSSION

Identifying Trap States. The first step in modeling a SurFET is identifying the trap states introduced in the silicon band gap by the adsorbed molecules. We determine these energy levels using *ab initio* calculations. The molecules discussed here are mostly benzene-based. The direct attachment chemistry of benzene rings onto silicon follows the work described in ref 20. The results are summarized in Figure 1. Our calculations are performed using density functional theory (DFT), and computational details are provided in Supporting Information. Once we obtain the energy levels of the silicon–molecule cluster, we identify the trap states that are localized primarily on the molecules *versus* the channel states that are delocalized over the silicon atoms (Figure 3). For aniline, we find three such levels in the band gap (Figure 1).

Simulating Current: Trap Fingerprints in Telegraph Noise. We will now analyze the dynamics of the trap states under an applied gate bias and explore their scattering signature on the output channel current. A positive gate voltage pushes the levels down, filling them sequentially as they enter the conduction window around the quasi-Fermi energy of the channel, set by

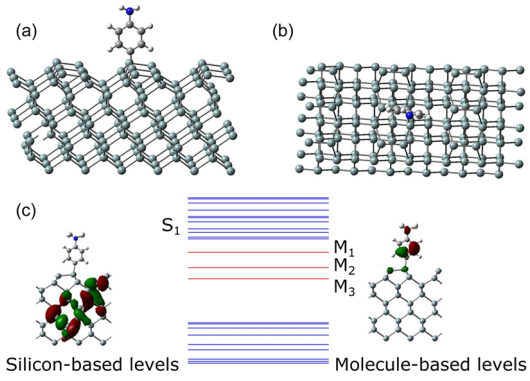

Figure 3. (a) Side and (b) top views of the optimized structure for aniline radical attached to a silicon dimer on a Si(100)-(2 × 1) slab H-passivated at the bottom. After we determined the optimized structure of the molecule–silicon system and obtained the bandstructure, we plotted the wave functions of the states that we were interested in. (c) This visualization of the wave functions shows us how the suite of cluster levels separates into silicon-based (blue S-states) localized on the Si cluster and molecule-based (red M-states) localized on the aniline molecule.

a small applied source to drain bias. In order to see resonant random telegraph signals, both the channel and the trap must align with the Fermi level at the same gate voltage. The levels and the channel move with gate voltage at very different rates, with the transfer factors varying with distance from the gate (Figure 4), an effect that can be enhanced in a nanowire channel with faster spatial variations in voltage profile.[19] Figure 4a shows how the bands bend upon application of a gate voltage, with the traps eventually slipping past the channel band-edge into resonance, thereby initiating the RTS sequence.

For a given energetic location of a trap state, we can write down its steady-state occupancy, assuming the trap is in equilibrium with its surroundings. Since the electron conduction occurs on time scales much faster than the trap dynamics, we can separately solve for the temporal evolution of the trap states using Monte Carlo techniques. We then include the dynamical effects through their instantaneous Coulomb effect onto the channel current, evaluated using a *steady-state* nonequilibrium Green's function (NEGF)-based quantum transport formalism.[21] The time axis is converted into

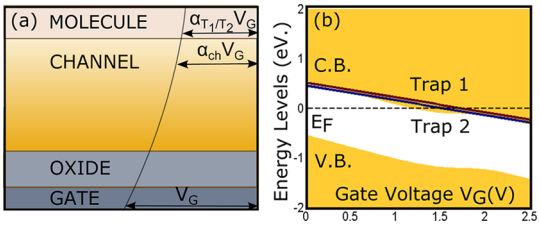

Figure 4. (a) Schematic band diagram of the SurFET, determined by the gate transfer factor α set by the doping. (b) Calculated evolution of the trap levels and channel conduction and valence bands under gate bias shows how the gate factors affect their movement, bringing them into resonance with the Fermi level and initiating the RTS.

a voltage axis using the voltage scan rate. For the stochastic trap dynamics, we can calculate the individual capture and emission times, which have both a spatial and a spectral component. The spectral component $\tau_{(c/e)}$, assuming detailed balance, is

$$\hbar/\tau_c = \gamma_t F(\varepsilon_t - \alpha_G V_G - \alpha_D V_D)$$

$$\hbar/\tau_e = \gamma_t[1 - F(\varepsilon_t - \alpha_G V_G - \alpha_D V_D)] \qquad (1)$$

where γ_t is the energy-dependent trap state broadening determined by a Fermi's Golden Rule estimate involving the overlap matrix elements between the molecule and silicon wave functions. The dimensionless parameters α_G and α_D denote the capacitive transfer factors between applied and local potentials at the gate and drain electrodes, respectively. Both the capacitive coupling α and the resistive coupling terms γ_t depend on the location of the trap relative to the electrodes (in a distributed circuit model or a matrix NEGF treatment, only specific site-coupling terms are nonzero). Under these conditions, the trapping time is given approximately by the time for the electron to drift or diffuse to the location of the trap, plus the time for it to get trapped locally. Finally, the trap occupancy function F is given by the modified Fermi–Dirac distribution $F(\varepsilon) = [1 + g\exp[(\varepsilon - \varepsilon_F)/(k_B T)]]^{-1}$, where the g-factor stands for spin-degeneracy of the trap energy level.

The unique transfer characteristic (I_{ds}–V_{ds}) is modeled using NEGF coupled with the stochastic trap dynamics near resonance. The time dependence of the dot occupancy over a time step dt can be extracted from a Monte Carlo simulation[6] with the capture probability dt/τ_c and emission probability dt/τ_e obtained earlier. The trap energies extracted from DFT are fed into a transport solver based on the above equations, generating stochastic switching in the current–time and current–voltage functions. While NEGF models are widely used for computing current flow, getting the RTS-mediated blocking accurately requires stochasticity, self-consistency, and most significantly self-interaction correction. In order to obtain cleaner data, the time traces are Fourier transformed to get a power spectral density (PSD) followed by filtering

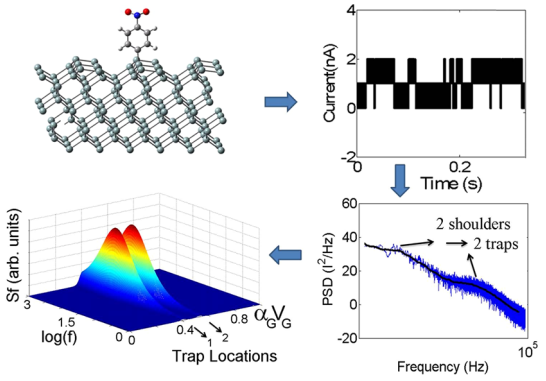

Figure 5. Typical time trace (top right) generated by a molecule-attached SurFET (top left), Fourier transformed (bottom right) to extract the power spectral density. The Gaussian-filtered PSD shows shoulders unique to the number and position of the traps, specifically, the corner frequencies set by the trap energies. Multiplying the spectrum by frequency removes the 1/*f* tail, yielding a shape function (bottom left) on a f–V_G plot with peaks corresponding to the trap levels.

using a Gaussian filter. The result shows clear shoulders arising from individual traps unique to the molecule, superposed on a 1/*f* noise background (Figure 5).

The power spectrum for multitrap RTS shows shoulders that merge into each other and are not easily distinguishable.[11] Multiplying the PSD by the frequency eliminates the 1/*f* tail and generates peaks at the corner frequencies of the three traps, following the relation (Supporting Information)

$$S(f, V_G)f = [4(\Delta I)^2]\frac{\beta(V_G)}{[1+\beta(V_G)]^2}\frac{f/f_c(V_G)}{1+f^2/f_c^2(V_G)} \qquad (2)$$

where ΔI is the change in current when the channel is blocked or released, $\beta = \tau_c/\tau_e$, and f_c is the corner frequency, defined as $f_c = 1/\tau_c + 1/\tau_e$.

While Sf maximizes at $f = f_c$ along the frequency axis, those peaks maximize at $\beta(V_G) = 1$ along the gate voltage axis; $\beta = 1$ identifies the points at which *the traps cross the Fermi level*. On a frequency–voltage colormap, we can directly read out from the voltage axis the energy locations of the suite of trap states (scaled by a gate transfer factor) and from the frequency axis their relevant broadening parameters. The number and location of the peaks provides detailed information about the trap states created within the band gap and serves as a unique fingerprint or molecular barcode. Figure 1 demonstrates proof-of-concept specificity of the current-noise-based characterization tool we envision, showing clearly that the PSDs are distinct for four similar molecules with slightly different end groups.

The previous sections developed the underlying equations for RTS as a route to characterizing molecular adsorbates with a backgated FET. Proper designing is essential to make this process efficient, for instance, an optimal doping so that we see large increases in conductance and yet enjoy an appreciable Debye

length from the gate. The microscopic equations we described apply for a range of trapping phenomena, from independent traps to traps that merge into a 1/*f* Hooge's law, including nonresonant multiphonon scattering processes for filling and emptying (Supporting Information). We can use these equations to extract information about the critical noise statistics directly from the PSD colormap.

For a two-state noise given by a specific capture or emission time, a set of independent random multiple trapping events satisfy Poissonian statistics. The probability of observing k jumps in the time interval T is given by $P(k,T) = (\lambda T)^k e^{-\lambda T}/k!$, where λ is the mean rate

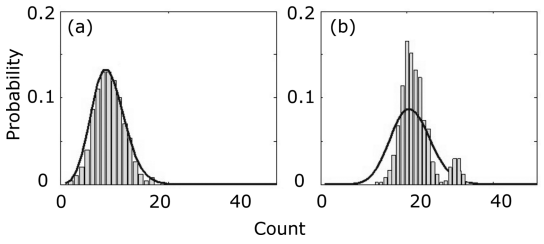

Figure 6. Full counting probability function for traps transitioning from the empty state to the filled state in 1 s. The bars represent the statistics for the simulated data, and the solid line is an ideal Poissonian fit. (a) This is the case for traps that are independent of each other and are uncorrelated; the statistics of such traps follow the ideal Poisson distribution, while (b) shows significant departure from the ideal Poissonian statistics, indicating correlation between traps. Such a deviation is seen in refs 22 and 19, where the authors observe non-Poissonian correlated random telegraph signal from the interaction of two individual defects in a carbon nanotube transistor.

of transitions per second. Our NEGF simulations for uncorrelated traps show such a Poissonian distribution in Figure 6a. In the past, a deviation from Poisson statistics was one way to identify correlation effects among traps.[22] In this section, we will show how the colormap extracted from the current noise can provide a more direct and detailed insight into such intertrap interactions.

We focus on transport data presented in ref 19, which shows a pronounced, notch-like drop in current over a small bias window (Figure 7a) atop a broader, smoother conductance dip typical of ambipolar nanotube FETs. The notch was found to shift reproducibly with bias V_{ds}. Closer examination reveals trapping and detrapping events on both sides of the notch. In ref 19, we attributed this RTS-flanged window to the interaction between two traps. In our model, the current blockade induced by one trap, responsible for the initial drop in current at the leading edge of the window, fully reversed when a second trap was activated, with the latter Coulomb blocking the first trap and unblocking the channel as a result. An NEGF calculation with Hubbard interactions among the traps and the channel yielded a great semiquantitative match with the observed $I-V$ and was used to extract the spatial locations within the oxide of the two traps responsible for the anomalous behavior. Figure 7b shows the NEGF-calculated dynamics of the traps and the CNT conduction band-edge relative to the Fermi energy. Figure 6b shows the counting statistics for the traps, showing significant departure from the ideal Poissonian statistics, indicating correlation between traps.

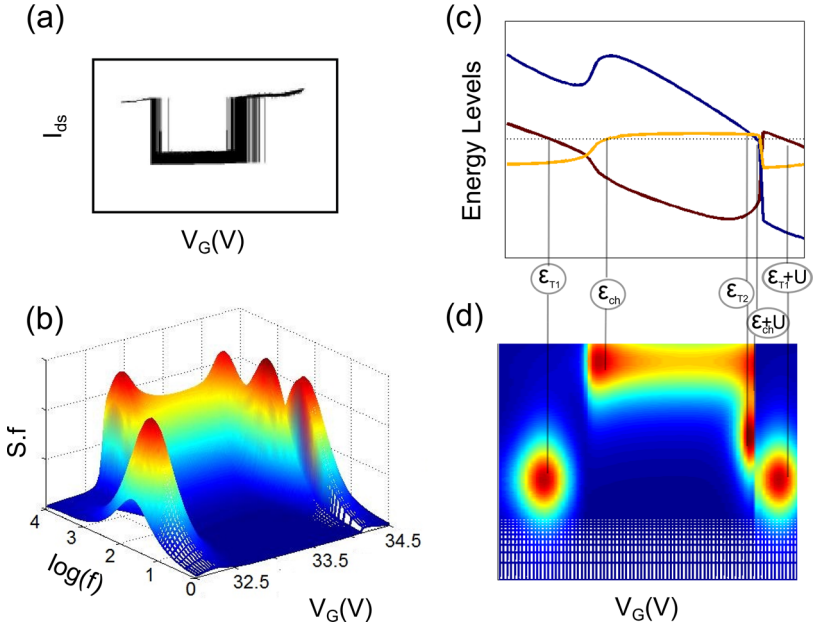

Figure 7. With correlated trap interaction, as embedded in the measured noise data (a) for a CNTFET,[19] the plot of PSD (multiplied by *f*) *vs* gate voltage is complicated, generating multiple peaks for each trap, shown in (b,d). The positions of the peaks can give us a snapshot of the level interplay and movement. (c) NEGF-simulated evolution of levels, calibrates very well with the extracted spectral data in (d). While (c) is based on a speculative theoretical model, (d) is directly extracted from a Fourier analysis of the time-resolved $I-V$ curves, showing us a clear picture of the trap interactions and locations and validating our theoretical model.

The frequency–voltage colorplot provides a direct way to validate our model. From the RTS signals, we can extract the PSD and multiply by the frequency to eliminate the 1/*f* tails. Plotting this product *versus* frequency and gate voltage provides a comprehensive picture of the occupied states at the Fermi energy (Figure 7c,d), which matches up very well with the model proposed earlier[19] (Figure 7b). We can directly "see" the first trap getting populated at lower voltage, pushing the channel out and initiating the window in the $I-V_G$. The channel hovers just above the Fermi energy until the second trap enters the conduction diagram, whereupon the first trap is repelled and the channel as a result is pulled back in, terminating the window. The colorplot gives us a snapshot of the trap interactions and allows us to identify the precise energies of the traps.

CONCLUSIONS

We provide a proof-of-concept for reagentless, real-time detection of single molecular spectra based on correlated quantum scattering, with reduced false positives and large signal-to-noise ratios. The RTS-based mechanism, coupled with other characterization techniques, can scan an entire "molecular barcode" to separate electrically interesting molecules from uninteresting ones. The fabrication of this novel nanosensor is similar to a standard ChemFET from a lithographic point of view, although it needs a solid-state environment for Coulomb blockade and specialized surface functionalization schemes to maximize wave function overlap with the channel. We develop a unified model, which can be used as a tool to study single and multitrap dynamics, their interactions in devices, and characterize and localize individual molecular impurities. As an illustrative example, we demonstrate the molecule-specific noise spectra of four benzene-based adsorbates on silicon transistors, as well as snapshots of intertrap interactions directly readable from a frequency–voltage colormap. The novelty in the analysis in this paper is that the analysis is done in the frequency domain while simultaneously resonating with a gate voltage. This will work if there are a few resonant trap states with good chemical bonds and we see clear signatures. The quasi-ballisticity of electron transport in today's nanotransistors makes them considerably more sensitive to surface processes, while enabling the deliberate engineering of few (often one or none) adsorbates or ordered arrays of molecular adsorbates through self-assembly.

METHODS

Our calculations are performed using DFT, as implemented in the program Gaussian 98[23] using the Becke three-parameter Perdew–Wang (B3PW91) hybrid functional. This functional uses the nonlocal three-parameter Becke[24] exchange functional (a combination of the generalized gradient approximation (GGA) Becke 1988[25] functional with the exchange calculated by the Hartree–Fock method[26] using Kohn–Sham molecular orbitals) and the nonlocal correlation provided by Perdew/Wang in 1991.[27,28] We use the valence double-ζ 6-31G* basis set for carbon, nitrogen, oxygen, and hydrogen atoms[29] and the LANL2DZ basis,[30–32] which includes effective core potentials for the 1s, 2s, and 2p shells of silicon. Geometry optimizations were carried out using DFT as implemented in the Vienna ab initio simulation package (VASP).[33,34] The atoms were represented using plane wave basis sets, and the PW91 form of the GGA functional was used to carry out gradient-corrected calculations. The unit cell of Si(100) slab had nine atomic layers, and the dangling bonds on the lower surface were passivated with hydrogen atoms. The lowest four layers of silicon were kept fixed, while the rest of the atoms were relaxed to get the optimized structure.

Conflict of Interest: The authors declare no competing financial interest.

Acknowledgment. The authors would like to thank Keith Williams, John Bean, Lin Pu, and Lloyd Harriott for useful discussions. This work was supported by DARPA-AFOSR, NSF-NIRT, and NSF-CAREER awards.

Supporting Information Available: Additional materials as discussed in text. This material is available free of charge *via* the Internet at http://pubs.acs.org.

REFERENCES AND NOTES

1. Kunz, R. R.; Gregory, K. C.; Hardy, D.; Oyler, J.; Ostazeski, S. A.; Fountain, A. W., III. Measurement of Trace Explosive Residues in a Surrogate Operational Environment: Implications for Tactical Use of Chemical Sensing in C-IED Operations. *Anal. Bioanal. Chem.* **2009**, *395*, 357–369.
2. Willis, C. M.; Church, S. M.; Guest, C. M.; Cook, W. A.; McCarthy, N.; Bransbury, A. J.; Church, M. R. T.; Church, J. C. T. Olfactory Detection of Human Bladder Cancer by Dogs: Proof of Principle Study. *BMJ* **2004**, *329*, 712–717.
3. Patolsky, F.; Zheng, G.; Lieber, C. M. Nanowire-Based Biosensors. *Anal. Chem.* **2006**, *78*, 4260–4269.
4. Kong, J.; Franklin, N. R.; Zhou, C.; Chapline, M. G.; Peng, S.; Cho, K.; Dai, H. Nanotube Molecular Wires as Chemical Sensors. *Science* **2000**, *287*, 622–625.
5. Hu, J.; Odom, T. W.; Lieber, C. M. Chemistry and Physics in One Dimension: Synthesis and Properties of Nanowires and Nanotubes. *Acc. Chem. Res.* **1999**, *32*, 435–445.
6. Vasudevan, S.; Walczak, K.; Kapur, N.; Neurock, M.; Ghosh, A. W. Modeling Electrostatic and Quantum Detection of Molecules. *IEEE Sens. J.* **2008**, *8*, 857–862.
7. Lang, D. Deep-Level Transient Spectroscopy: A New Method To Characterize Traps in Semiconductors. *J. Appl. Phys.* **1974**, *45*, 3023–3032.
8. Ralls, K.; Skocpol, W.; Jackel, L.; Howard, R.; Fetter, L.; Epworth, R.; Tennant, D. Discrete Resistance Switching in Submicrometer Silicon Inversion Layers: Individual Interface Traps and Low-Frequency (1/*f*?) Noise. *Phys. Rev. Lett.* **1984**, *52*, 228–231.
9. Dekker, C.; Scholten, A.; Liefrink, F.; Eppenga, R.; Van Houten, H.; Foxon, C. Spontaneous Resistance Switching and Low-Frequency Noise in Quantum Point Contacts. *Phys. Rev. Lett.* **1991**, *66*, 2148–2151.
10. Neugroschel, A.; Sah, C.-T.; Carroll, M. S. Random Telegraphic Signals in Silicon Bipolar Junction Transistors. *Appl. Phys. Lett.* **1995**, *66*, 2879–2881.
11. Amarasinghe, N. V.; Çelik-Butler, Z.; Zlotnicka, A.; Wang, F. Model for Random Telegraph Signals in Sub-micron MOSFETS. *Solid-State Electron.* **2003**, *47*, 1443–1449.
12. Xiao, M.; Martin, I.; Yablonovitch, E.; Jiang, H. Electrical Detection of the Spin Resonance of a Single Electron in a Silicon Field-Effect Transistor. *Nature* **2004**, *430*, 435–439.
13. Yin, C.; Rancic, M.; de Boo, G. G.; Stavrias, N.; McCallum, J. C.; Sellars, M. J.; Rogge, S. Optical Addressing of an Individual Erbium Ion in Silicon. *Nature* **2013**, *497*, 91–94.

14. Liu, F.; Bao, M.; Kim, H.-j.; Wang, K. L.; Li, C.; Liu, X.; Zhou, C. Giant Random Telegraph Signals in the Carbon Nanotubes as a Single Defect Probe. *Appl. Phys. Lett.* **2005**, *86*, 163102–163102.
15. Clément, N.; Nishiguchi, K.; Fujiwara, A.; Vuillaume, D. One-By-One Trap Activation in Silicon Nanowire Transistors. *Nat. Commun.* **2010**, *1*, 92–99.
16. Zheng, G.; Gao, X. P.; Lieber, C. M. Frequency Domain Detection of Biomolecules Using Silicon Nanowire Biosensors. *Nano Lett.* **2010**, *10*, 3179–3183.
17. Goldsmith, B. R.; Coroneus, J. G.; Kane, A. A.; Weiss, G. A.; Collins, P. G. Monitoring Single-Molecule Reactivity on a Carbon Nanotube. *Nano Lett.* **2008**, *8*, 189–194.
18. Guo, Q.; Kong, T.; Su, R.; Zhang, Q.; Cheng, G. Noise Spectroscopy as an Equilibrium Analysis Tool for Highly Sensitive Electrical Biosensing. *Appl. Phys. Lett.* **2012**, *101*, 093704–093704.
19. Chan, J.; Burke, B.; Evans, K.; Williams, K. A.; Vasudevan, S.; Liu, M.; Campbell, J.; Ghosh, A. W. Reversal of Current Blockade in Nanotube-Based Field Effect Transistors through Multiple Trap Correlations. *Phys. Rev. B* **2009**, *80*, 033402–033405.
20. He, T.; He, J.; Lu, M.; Chen, B.; Pang, H.; Reus, W. F.; Nolte, W. M.; Nackashi, D. P.; Franzon, P. D.; Tour, J. M. Controlled Modulation of Conductance in Silicon Devices by Molecular Monolayers. *J. Am. Chem. Soc.* **2006**, *128*, 14537–14541.
21. Datta, S. *Quantum Transport: Atom to Transistor*; Cambridge University Press: Cambridge, UK, 2005.
22. Liu, F.; Wang, K. L. Correlated Random Telegraph Signal and Low-Frequency Noise in Carbon Nanotube Transistors. *Nano Lett.* **2008**, *8*, 147–151.
23. Frisch, M.; Trucks, G.; Schlegel, H.; Scuseria, G.; Robb, M.; Cheeseman, J.; Zakrzewski, V.; Montgomery, J., Jr.; Stratmann, R.; Burant, J.; *et al. Gaussian 98*, revision A.6.; Gaussian. Inc.: Pittsburgh, PA, 2008.
24. Becke, A. D. A New Mixing of Hartree−Fock and Local Density-Functional Theories. *J. Chem. Phys.* **1993**, *98*, 1372–1377.
25. Becke, A. D. Density-Functional Exchange-Energy Approximation with Correct Asymptotic Behavior. *Phys. Rev. A* **1988**, *38*, 3098–3100.
26. Szabo, A.; Ostlund, N. S. *Modern Quantum Chemistry: Introduction to Advanced Electronic Structure Theory*; Dover Publications: Mineola, NY, 1989.
27. Perdew, J. P.; Chevary, J.; Vosko, S.; Jackson, K. A.; Pederson, M. R.; Singh, D.; Fiolhais, C. Atoms, Molecules, Solids, and Surfaces: Applications of the Generalized Gradient Approximation for Exchange and Correlation. *Phys. Rev. B* **1992**, *46*, 6671–6687.
28. Perdew, J. P.; Wang, Y. Accurate and Simple Analytic Representation of the Electron-Gas Correlation Energy. *Phys. Rev. B* **1992**, *45*, 13244–13249.
29. Hehre, W. J.; Ditchfield, R.; Pople, J. A. Self-Consistent Molecular Orbital Methods. XII. Further Extensions of Gaussian-Type Basis Sets for Use in Molecular Orbital Studies of Organic Molecules. *J. Chem. Phys.* **1972**, *56*, 2257–2261.
30. Hay, P. J.; Wadt, W. R. *Ab Initio* Effective Core Potentials for Molecular Calculations. Potentials for the Transition Metal Atoms Sc to Hg. *J. Chem. Phys.* **1985**, *82*, 270–283.
31. Wadt, W. R.; Hay, P. J. *Ab Initio* Effective Core Potentials for Molecular Calculations. Potentials for Main Group Elements Na to Bi. *J. Chem. Phys.* **1985**, *82*, 284–298.
32. Hay, P. J.; Wadt, W. R. *Ab Initio* Effective Core Potentials for Molecular Calculations. Potentials for K to Au Including the Outermost Core Orbitals. *J. Chem. Phys.* **1985**, *82*, 299–310.
33. Kresse, G.; Furthmüller, J. Efficient Iterative Schemes for *Ab Initio* Total-Energy Calculations Using a Plane-Wave Basis Set. *Phys. Rev. B* **1996**, *54*, 11169–11186.
34. Kresse, G.; Furthmüller, J. Efficiency of *Ab-Initio* Total Energy Calculations for Metals and Semiconductors Using a Plane-Wave Basis Set. *Comput. Mater. Sci.* **1996**, *6*, 15–50.